Study of Reynolds number effect on turbulent boundary layer near the separation

A Dróżdż[1] **and W Elsner**[1]

[1] Częstochowa University of Technology, Faculty of Mechanical Engineering and Computer Science, Armii Krajowej 21, 42-200 Czestochowa, Poland

E-mail: welsner@imc.pcz.czest.pl

Abstract. The paper deals with the experimental analysis of strong decelerated turbulent boundary layer developed on a flat plate. The special design of the test section equipped with perforated, movable upper wall allow to generate on the bottom wall turbulent boundary layer, which is at the verge of separation. The objective of the work is to examine the effect of Reynolds number on non-equilibrium boundary layer. A momentum thickness Reynolds number at the inlet to a test section was in the range from 6300 to 10150 what was achieved by varying wind tunnel speed. The emphasis is on the analysis of the streamwise Reynolds stress and mean velocity profiles and on related scaling issues problem. It was found that for the same external conditions defined by the pressure gradient coefficient *Cp* the effect of Reynolds number close the wall is seen even for such a narrow range of Reynolds number. In particular, the shape factor revealed more flow resistance on separation with increase in Reynolds number. The difference where observed mainly at the beginning of incipient detachment, where there is a drop of turbulence activity near the wall while it reaches a maximum value in the outer region.

1. Introduction

Although a significant amount of research has been devoted to understanding canonical flat plate zero pressure gradient boundary layer, it is not the case for adverse pressure gradient boundary layers and even more when the flow is approaching separation. The most common problem in the similarity analysis is the Reynolds number effect [1]. For zero pressure gradient boundary layer it is known that scaling parameters of classical inner or outer scaling are a function of Reynolds number. It is not the case for more complex system, where additional length or time scales are introduced by the geometry or system dynamics. These scales do not develop in the same manner with Reynolds number as the traditional ones [1]. It is the reason why the non-linear effect is observed, what is seen by the rapid decrease of near wall viscous length scale and week variation of the outer length scale with Reynolds number. This is particularly important when trying to analyze adverse pressure gradient (APG) flows and to predict the separation location on curved surface, where due to considerable change of the wall shear in the streamwise direction, the turbulence cannot be characterized solely in terms of local parameters [2]. In the case when a boundary layer approaches separation the mean velocity inflectional profiles produce conditions for emergence of large eddies which interacts with those already present in the flow [3]. A different process of decay of those eddies may be responsible for the lack of similarity of those non-equilibrium flows.

Difficulties in scaling of APG wall-bounded flows may also emerge from amplitude modulation effect of small scales by large scale structures, which was elucidated by skewness changes of filtrated

velocity small and large scale signals [4]. The physical phenomenon of amplitude modulation is still unknown, but it seems that it influences the wall-normal momentum transport by the changing the convection velocity of small scales [5]. If so, this may postpone separation with rise of the Reynolds number.

In the most available experimental research with APG flows there is a lack of canonical setup [6]. The paper is an attempt to fill this gap. The main motivation of the present study is to verify the effect of Reynolds number at matched conditions of pressure gradient leading to detachment and to analyze how it influence the scaling of mean and fluctuating velocity profiles.

2. Experimental facility and measurement technique

The experiment was performed in an open-circuit wind tunnel, where the turbulent boundary layer was developed along the flat plate, which was 6870 mm long. The wind tunnel is designed with large dimension settling chamber and three contraction sections, which allows to achieve free stream turbulence intensity below 1% at the inlet plane. In order to bypass laminar-turbulent transition, the tripping of boundary layer after the leading edge was used. The inlet rectangular channel with a length of 5.035 m located upstream the proper test section has two pairs of suction gaps aimed to control the two-dimensionality of the flow by minimizing of boundary layers on the side walls. In order to reduce the effect of secondary vortices developing along rectangular channels the triangular corner inserts were used in the whole inlet channel. A slight inclination of the upper wall helped to keep zero pressure gradient (ZPG) conditions at the at the entire length of this section.

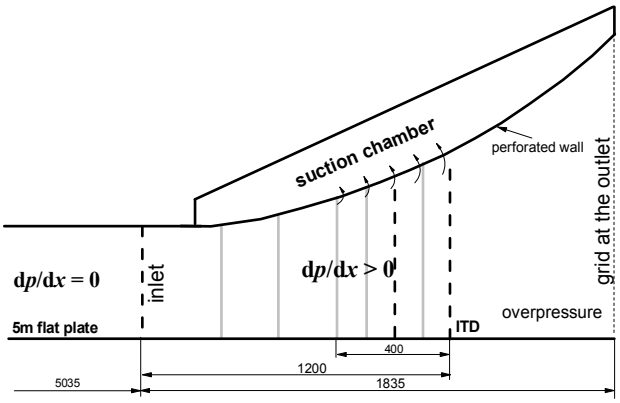

Figure 1. Test section geometry

The specially design test section located at the end of the wind-tunnel (see figure 1) is equipped with perforated, movable upper wall. Computer-controlled suction system equipped with a low power axial compressor allows for smooth adjustment of the amount of the exhausted air from the top of the wall. By playing with the shape and position of the upper wall as well with the suction flux it is possible to generate wide range of pressure gradient conditions, while at the inlet channel the zero pressure gradient conditions were secured. The static pressure in the test section is increased by the throttling at the outlet of the test section. For certain pressure conditions it is possible to generate on the bottom wall the turbulent boundary layer, which is at the verge of separation.

Static pressure measurements were done through pressure holes of 0.5 mm dia, drilled along the side line along the streamwise direction, from -700 to 1750 mm of the x coordinate where zero is set at the inlet plane (see Fig. 1). The spacing of pressure taps was equal 50 mm. Pressure differences were measured by means of DATA INSTRUMENTS DCXL01DN pressure transducer connected to KULITE D486 amplifier. The mean relative error of pressure measurements equals 2%.

The velocity measurements were performed with hot-wire anemometry CCC developed by Polish Academy of Science in Krakow. A single hot-wire probe of a diameter d = 3 μm and length l = 0.4 mm was used. In the experiment for each case the wire length was always below 20 in inner variables as it was recommended by Ligrani and Bradshaw [15]. The hot-wire bridge was connected to a 16 bit

PC card. Acquisition was maintained at frequency 25 kHz with 30 s sampling records. The ambient conditions were carefully controlled during the measurements. In the course of a single profile measurement the scatter of ambient temperature at the end of the test section did not exceed ±0.2°. In case when the measured temperature was different from temperature during calibration, the temperature correction of CTA voltage was used by Jorgensen [7]. At the same time the free-stream velocity was monitored by the means of a Prandtl's tube.

The facility is equipped with the computer-controlled 2D traversing system (in streamwise and wall-normal direction). The traverse carriage was driven over the maximum displacement of 180 mm by a servo motor. Uncertainty of the drive step in wall normal direction was 0.001 mm with the smallest step equal 0.01 mm, while in the streamwise direction the uncertainty was equal drive step of 0.37 mm.

To have the verified reference friction velocity u_τ along the flow except the Clauser plot method, the fringe skin friction (FSF) technique was also applied [8]. This method, in contrast to hot-wire technique, does not require any assumptions about the form of velocity profile and is very simple and reliable. It is based on the relationship between the thinning of an oil film deposited on the surface exposed to the flow and the local shear stress. In the experiment described in [9] SOX Whitecroft Lighting sodium lamp, emitting the monochromatic light of the wavelength λ = 0.5893 μm, for illuminating the oil-film was used. The relative error was in the range of 1% for maximal of skin friction value estimated by FSF technique. The shear stresses were compared with the ones obtained by modified Clauser plot method with satisfactory results with standard parameters of logarithmic law of the wall κ = 0.38 and B = 4.1 taken from hot-wire measurements up to x = 700 mm [10]. The u_τ values used in the paper were obtained based on FSF method above location of x = 700 mm apart from the case of 15 m/s, which was obtained by scaling using the inlet value for each Reynolds number.

3. Test cases description

Flow parameters determined in core flow at the inlet plane to test section (i.e. 5035 mm downstream the flat plate leading edge), located in the zero pressure gradient area, are the mean velocity U ≈ 10, 15 and 20 m/s and turbulence intensity Tu < 1%. The inlet Reynolds number based on friction velocity and boundary layer thickness was equal 1900, 2600 and 3300 respectively. To activate the side suction gaps the overpressure 15 Pa was set at the inlet plane. Basic inlet parameters have been summarized in Table 1, where Tu is turbulence intensity, U_{in} mean velocity outside of TBL, u_τ friction velocity $u_\tau = \sqrt{\frac{\tau_w}{\rho}}$, θ momentum loss thickness and $Re_\theta = \frac{U_{in}\theta}{\nu}$ is Reynolds number, where ν is the kinematic viscosity.

Table 1. Inlet conditions of ZPG turbulent boundary layer.

	Tu [%]	U_{in} [m/s]	u_τ [m/s]	θ [mm]	Re_θ [-]
□	<1%	10	0.72	8.26	6300
○	<1%	15	0.55	8.91	8200
Δ	<1%	20	0.37	10.3	10150

The grey vertical lines in Fig. 1 represent the positions where the measurements of velocity profiles were performed, while detailed comparison was done at three locations marked as dark dashed vertical lines. In the last position the boundary layer has a features typical for Intermittent Transitory Detachment (ITD) defined by Simpson [11] as 20% of reversed flow. Measurements were performed for three different Reynolds number and perfectly matched distributions of pressure coefficient:

$$C_p = 1 - \left(\frac{U_\infty}{U_{\infty_0}}\right)^2, \quad (1)$$

shown in figure 2a, where $U_{\infty 0}$ is the mean inlet velocity. In figure 2b the Clauser-Rotta pressure gradient parameter β defined as:

$$\beta = \frac{\Delta}{u_\tau}\frac{dU_\infty}{dx}, \tag{2}$$

where $\Delta = \delta^* \frac{U_\infty}{u_\tau}$ and $\delta^*$is displacement thickness, is presented.

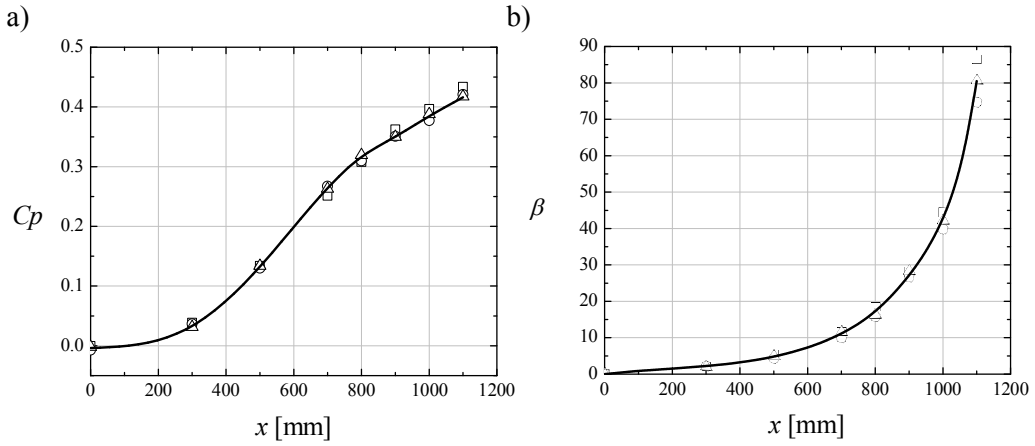

Figure 2. Distributions of the flow parameters: Pressure gradient parameter C_p a) and Clauser-Rotta pressure gradient parameter β b)

It is seen that, irrespective of different Reynolds number both C_p and β distributions matches well. This confirms that from the point of view of pressure gradient it was possible to get similar external conditions. For the completeness of data figure 3 presents the pressure and the pressure gradient distributions.

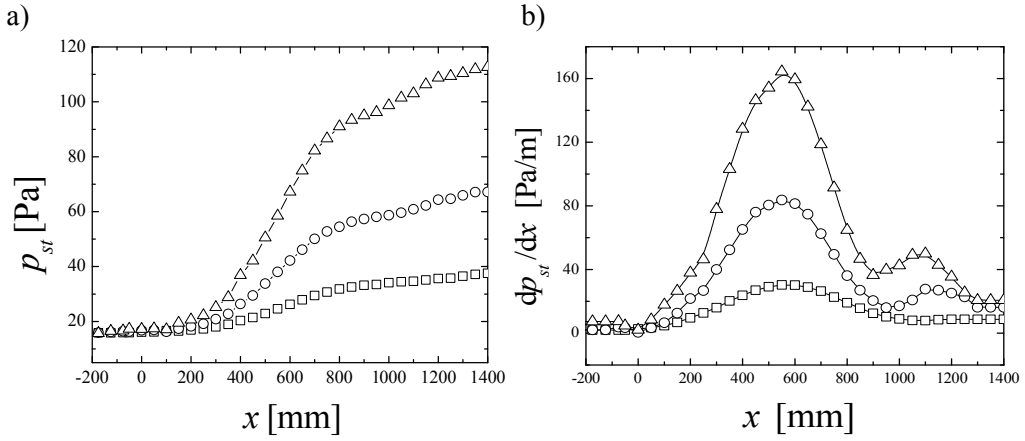

Figure 3. Pressure a) and pressure gradient b) distributions for analyzed range of *Re*.

It is seen that the shape of pressure gradient distribution at the wall varies slightly across the cases. In particular, the second maximum of pressure gradient (figure 3b) is placed at different position. This may be caused by interfering impact of separation on pressure measurements and must be clarified in the future.

4. Results

Data analysis starts with the inlet plane. Figure 4 shows the mean streamwise velocity profiles and streamwise Reynolds stresses presented in outer scaling (a) and 9b) and inner scaling (c) and (d). In the figure U_o is the outer scale velocity defined as $U_o = 2(U_\infty - U_{y=0.5\delta})$, which is similar to Zagarola-Smith scale [12].

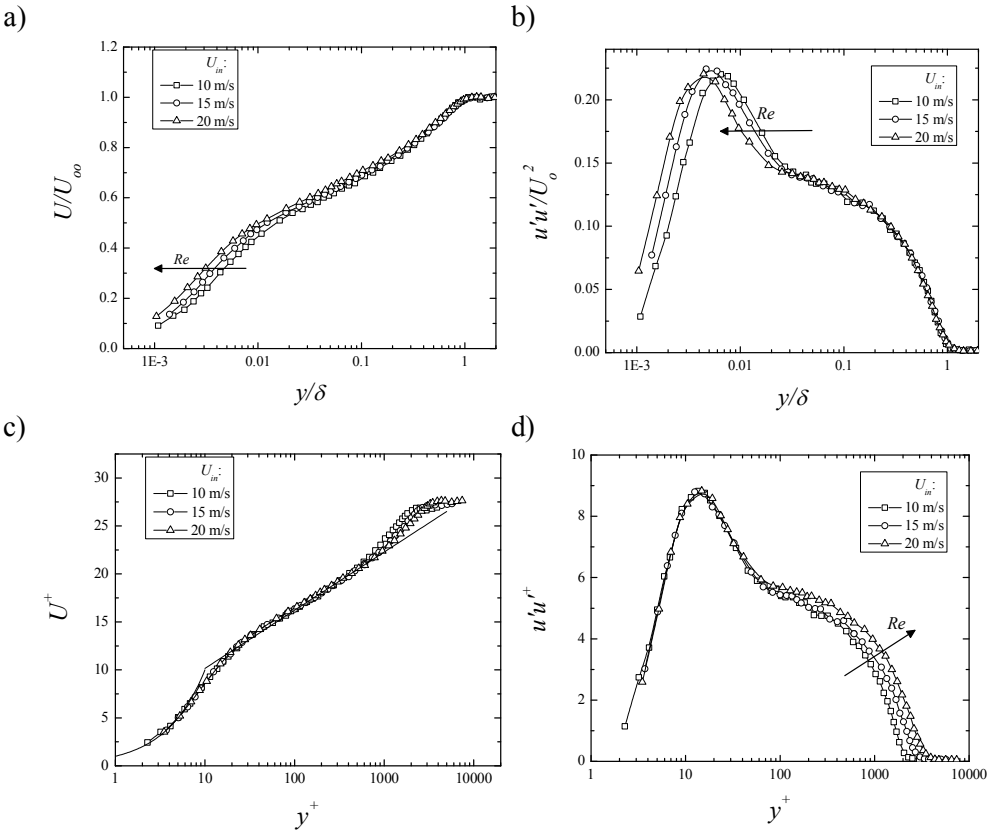

Figure 4. Mean velocity profiles in outer a) and inner variables c); streamwise Reynolds stress distributions in outer b) and inner variables d) at inlet location for analysed Reynolds numbers.

Scaling with outer variables aims to show the difference near the wall, while inner scaling reveal changes in the outer layer. In the figure the typical effect of Reynolds number is observed. Particularly there is an increase of log-layer range for mean profiles and increase of streamwise normal Reynolds stress in the outer region, which is related to the rise of a large scales energy in this region. For such a narrow range of Reynolds number the near wall peak reveal only minor increase of maximum what was also indicated by Marusic et al. [14].

Figure 5 presents the downstream evolution of the boundary layer thickness δ and shape factor $H=\delta^*/\theta$. While the inlet values behave as expected with increase of Reynolds number it is not the case for APG region. It is seen that in the direction of the flow and especially at the verge of separation the difference between δ values decreases. On the other hand, the reaction of shape parameter on *Re* is weaker. Nevertheless, in each case a strong almost linear increase of *H* from *x* = 700mm is seen, while the beginning of this growth delays with Reynolds number. Such a tendency in *H* is due to strong drop of mean momentum defect.

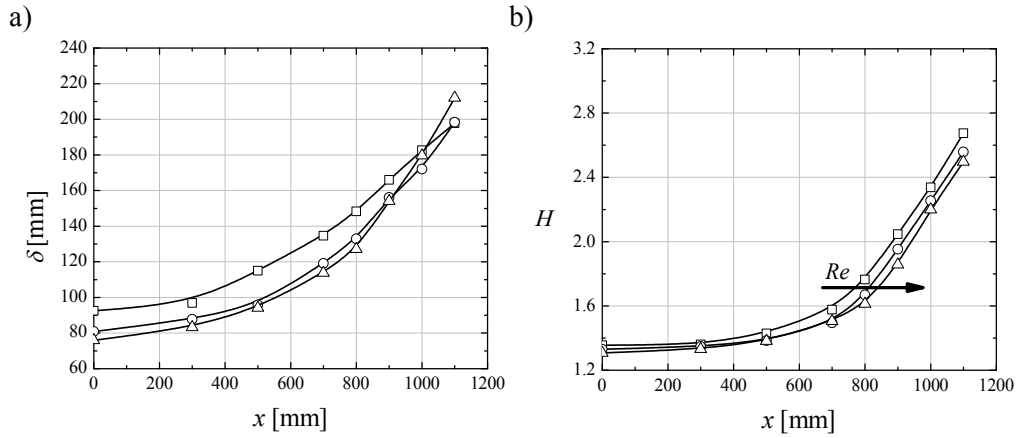

Figure 5. Distributions of the flow parameters: boundary layer thickness δ (a) and shape factor H (b)

Figure 6 presents the scaling of mean velocity and streamwise Reynolds stress profiles along the APG region for the largest Re number (Re_θ = 10150). Because the flow dynamics in separation region is dominated by outer layer large scale motions the scaling analysis were performed using outer variables introduced already in figure 4a-b.

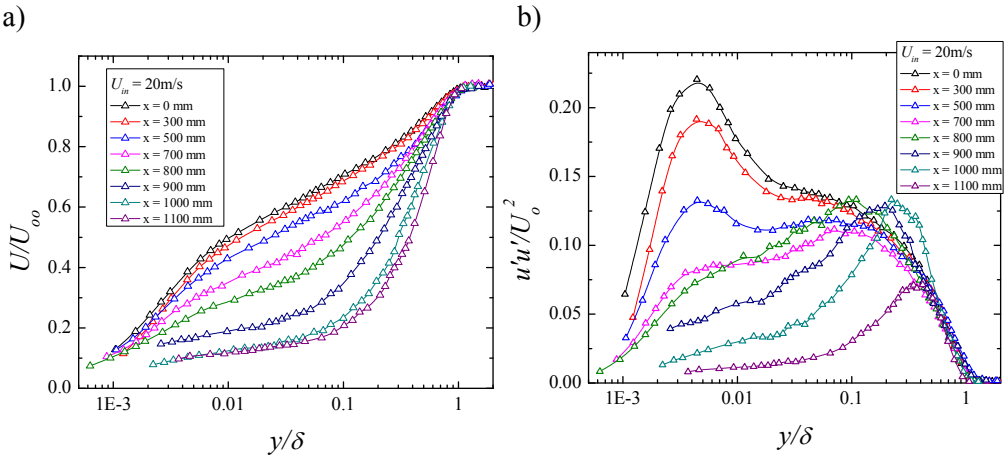

Figure 6. Mean velocity profiles (a) and streamwise Reynolds stress distributions (b) for 20 m/s case

In the downstream direction a strong deformation of velocity profile and the change of the shape of streamwise Reynolds stress can be noticed. The biggest difference between particular profiles appear near the wall. Approaching separation the near-wall peak decreases rapidly and vanishes near the separation. On the other hand, the rise of the outer peak is observed, which coincides well with the increase of dU/dy observed in figure 6a. In figure 6b the sharp increase in the value of $u'u'$ in the outer region close to separation is seen, what is due to the strong activity of large scale structures. It is clear from the above graphs that outer scaling fails in the adverse pressure gradient. This also indicates that the constant scaling factor throughout the boundary layer thickness is not appropriate for Reynolds stress profiles.

To compare the Reynolds number effect on APG boundary layer two different locations were chosen. First one is x = 900 mm with $\beta \approx 28$, where there is the greatest difference in the shape factor (see figure 5). The second one is the last measuring position x = 1100 mm with the highest pressure parameter $\beta \approx 80$. The comparison is presented in figure 7.

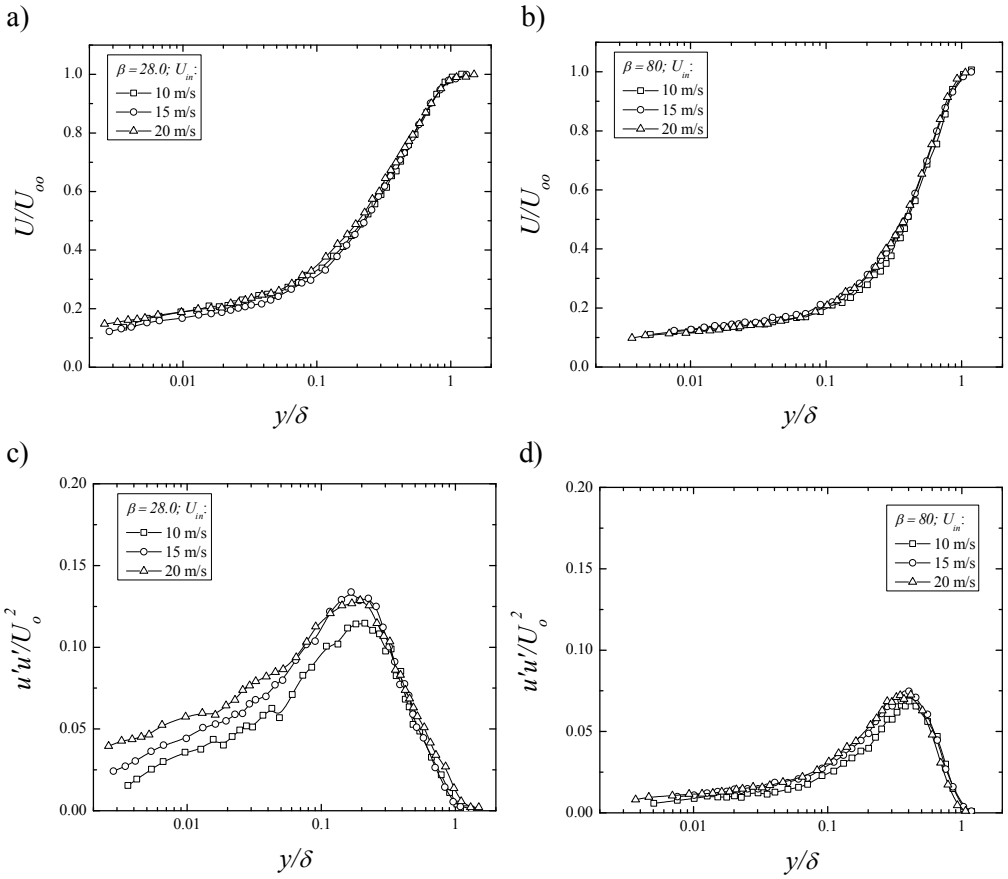

Figure 7. Mean velocity profiles a) and b) and streamwise Reynolds stress distributions b) and d) respectively for $\beta \approx 28$ and for $\beta \approx 80$

Despite that mean velocity profiles well overlaps (see figures 7a and 7b the difference is seen for *u'u'* especially close to the wall. This is more evident for the first location (x = 900 mm), where strong enhancement of the outer peak with the rise of Reynolds number is observed. It confirms the dominant role of the outer length scales and it is different to the observed behaviour for canonical zero pressure gradient flows visible in figure 4b. Surprisingly, the effect of Reynolds number decays at the last location. It is probably due to vanishing of small-scale turbulence and only large scales left to drive the flow. The growth of the outer peak, seen in figure 7c, may be also related to mentioned in the introduction amplitude modulation effect and the resulting changes of convection velocity of small scales which influences wall-normal momentum transport. The symptom of increased momentum transport is visible as the elevation of Reynolds stress near the wall (see figure 7c). It is not so clearly visible on mean profiles probably due to narrow range of Reynolds number.

5. Conclusions

The influence of Reynolds number on turbulent strong decelerated turbulent boundary layer developed on a flat plate was analysed. A momentum thickness Reynolds number at the inlet to a test section was in the range from 6300 to 10150.

It was found that for the same external conditions defined by the pressure gradient coefficient *Cp* the effect of Reynolds number close the wall is seen even for such a narrow range of Reynolds number. In particular, the shape factor revealed more flow resistance on separation with increase in Reynolds number. The difference where observed mainly at the beginning of incipient detachment, where there is a drop of turbulence activity near the wall while it reaches a maximum value in the outer region. The sharp increase in the value of *u'u'* in the outer region is probably due to the strong activity of large scale structures. The growth of the outer peak may be also related to mentioned in the introduction amplitude modulation effect and the resulting changes of convection velocity of small

scales which influences wall-normal momentum transport. Nevertheless the primary reason this phenomenon causes the failing of outer scaling methods. Surprisingly, the effect of Reynolds number decays at the last location, where the boundary layer has a features typical for Intermittent Transitory Detachment having 20% of reversed flow. It is probably due to vanishing of small-scale turbulence and only large scales left to drive the flow.

Acknowledgment
The investigations presented in this paper have been obtained with funding from Polish National Centre of Science within the grant DEC 2011/03/B/ST8/06401 as well as statutory fund BS 1-103-301/2015

References

[1] Degraaff D B, Webster D R and Eaton J K 1999 The effect of Reynolds number on boundary layer turbulence *Exp. Therm. Fluid Sci.* **18** 341–6
[2] Dróżdż A, Elsner W and Drobniak S 2015 Scaling of streamwise Reynolds stress for turbulent boundary layers with pressure gradient *Eur. J. Mech. B/Fluids* **49** 137–45
[3] Song S and Eaton J K 2004 Reynolds number effects on a turbulent boundary layer with separation, reattachment, and recovery *Exp. Fluids* **36** 246–58
[4] Mathis R, Marusic I, Hutchins N and Sreenivasan K R 2011 The relationship between the velocity skewness and the amplitude modulation of the small scale by the large scale in turbulent boundary layers *Phys. Fluids* **23** 121702
[5] Dróżdż A 2014 Influence of pressure gradient on streamwise skewness factor in turbulent boundary layer *J. Phys. Conf. Ser.* **530** 012061
[6] Gungor A G, Maciel Y, Simens M P and Soria J 2014 Analysis of a Turbulent Boundary Layer Subjected to a Strong Adverse Pressure Gradient *J. Phys. Conf. Ser.* **506** 012007
[7] Jorgensen F E 2002 *How to measure turbulence with hot-wire anemometers - a practical guide* ed Dantec Dynamics (Dantec Dynamics A/S, P.O. Box 121, Tonsbakken 16-18, DK-2740 Skovlunde, Denmark)
[8] Tanner L H and Blows L G 1976 A study of the motion of oil films on surfaces in air flow, with application to the measurement of skin friction *J. Phys. E.* **9** 194–202
[9] Dróżdż A, Elsner W and Drobniak S 2008 Application of oil-fringe interferometry for measurements of wall shear stress *Turbomachinery* **133** 103–10
[10] Dróżdż A, Elsner W and Sikorski D 2016 Skin Friction Measurements by Thin-Oil Film Interferometry in Turbulent Boundary Layer with Pressure Gradient *12th International Symposium On Compressor & Turbine Flow Systems Theory & Application Areas SYMKOM,* pp 18–9
[11] Simpson R L 1989 Turbulent Boundary-Layer Separation *Annu. Rev. Fluid Mech* **21** 205–34
[12] Zagarola M V. and Smits A J 1998 Mean-flow scaling of turbulent pipe flow *J. Fluid Mech.* **373** 33–79
[13] George W K and Castillo L 1997 Zero-pressure-gradient turbulent boundary layer *Appl. Mech. Rev.* **50** 689–730
[14] Marusic I, Mathis R and Hutchins N 2010 High Reynolds number effects in wall turbulence *Int. J. Heat Fluid Flow* **31** 418–28
[15] Ligrani P M and Bradshaw P 1987 Spatial resolution and measurement of turbulence in the viscous sublayer using subminiature hot-wire probes *Exp. Fluids* **5** 407–17